Discover Applied Sciences

Research

Activity of *Bambusa vulgaris* extract in reducing silver nanoparticles: evaluation against methylene blue organic pollutant and microbial agents

S. S. Prabula[1,6] · C. Hentry[1,6] · Saleh Al-Farraj[2] · P. Ram Kumar[3] · Mika Sillanpää[4] · M. Aravind[5]

Received: 19 October 2023 / Accepted: 4 March 2024
Published online: 18 March 2024

Abstract

This article presents an investigation focusing on successfully synthesising silver nanoparticles with zero valences. The synthesis involves utilising an extract from bamboo leaves, specifically those obtained from the *Bambusa vulgaris* species. X-ray diffraction, transmission electron microscopy, Fourier transform infrared, and ultraviolet–visible spectroscopy characterised the synthesised Ag nanomaterials. The X-ray diffraction pattern obtained from the collected samples confirms the presence of a face-centred cubic structure and a significant level of crystallinity. The studied materials had a spherical morphology, as determined by transmission electron microscopy analysis. The particle size was measured to be 22 nm. FT-IR analysis validates the presence of biomolecules in the leaf extract, which is accountable for the reduction of Ag^+ ions and subsequent stabilisation of Ag nanoparticles. Without chemical agents, the reduction of Ag ions to Ag was confirmed using UV–Vis spectroscopy. This analytical technique revealed a peak at 450 nm, indicating surface plasmon resonance. Photogenerated electron carriers can be inferred from a distinct and diverse set of photoluminescence spectra. The study also includes an analysis of the photocatalytic effectiveness of the synthesised silver nanoparticles, specifically in the breakdown of methylene blue (MB) dye. The efficacy of the silver nanoparticle (Ag NP) photocatalyst was assessed by examining the degradation process of a methylene blue dye solution in an aqueous medium under direct sunlight exposure. The experiment also evaluated the impact of catalyst dosage and dye concentration on the efficient degradation of MB dye. The investigation findings indicate that the optimal catalyst dosage and dye concentration were determined to be 0.015 mg/mL and 10 µM, respectively. Notably, the photocatalytic degradation process exhibited remarkable efficacy, with a peak efficiency of 94% after 120 min under direct solar irradiation. The experimental results suggest that the synthesised particles demonstrate a disintegration rate of 96% over 120 min when exposed to visible light. The utilisation of bio-processed silver nanoparticles has exhibited the achievement of phase purity during the manufacturing process, as well as an enhancement in catalytic efficacy. It implies that the synthesised technique offers a more advantageous option for producing nanoparticles on a large scale, potentially applicable in wastewater treatment at a broad level.

Article highlights

1. Bambusa vulgaris utilized for the synthesis of silver nanoparticles.

✉ M. Aravind, aravind-sh@nec.edu.in | [1]Department of Physics, St. Judes College, Thoothoor, Kanyakumari, Tamil Nadu 629176, India. [2]Department of Zoology, College of Science, King Saud University, Riyadh, Saudi Arabia. [3]Department of Chemistry, ThiagarajarCollege of Engineering, Thiruparankundram, Madurai, Tamil Nadu 625015, India. [4]Functional Materials Group, Gulf University for Science and Technology, 32093 Mubarak Al-Abdullah, Kuwait. [5]Department of Physics, National Engineering College, Kovilpatti, Tamil Nadu, India. [6]ManonmaniamSundaranar University, Abishekapatti, Tirunelveli, Tamil Nadu 627012, India.

2. Antibacterial and antibiofilm activities of AgNPs against *Pseudomonas aeruginosa* and *Staphylococcus aureus*.
3. Highest degradation efficency of 94% were observed.

Keywords Environmental research · Biosynthesis · Antibacterial activity · Bio-inspired nanoparticles

1 Introduction

Green nanotechnology is a method that focuses on creating nanomaterials in a sustainable and eco-friendly way. It aims to address the environmental and health issues associated with traditional synthesis methods. This field is dedicated to minimising hazardous chemicals, reducing energy consumption, and minimising waste generation during synthesis. Nanoparticles synthesised using green methods possess distinct properties and functionalities, rendering them highly promising for various applications, including healthcare, energy, agriculture, environmental remediation, and consumer products. For instance, they find applications in targeted drug delivery systems, antimicrobial coatings, pollution remediation, and renewable energy technologies. The biocompatibility and sustainability of green nanomaterials offer exciting opportunities to tackle global challenges while reducing environmental impacts. Exploring the significance of green nanotechnology and its diverse applications has the potential to shape a sustainable and technologically advanced future [1–5].

The expeditious production of noble metal nanoparticles has garnered significant interest because of their distinct and captivating features absent in the macroscopic phase. Metal nanoparticles possess a notable level of photocatalytic efficacy and have demonstrated potential in several biological applications [6]. Moreover, metal nanoparticles exhibit distinctive physical and chemical properties, making them a distinct class of materials that find extensive utility across various disciplines such as biomedicine [7], biosensing technology [8], catalysis [9], tissue engineering [10], food packaging [11], and environmental sciences. The synthesis approach, "chemical and physical," encompasses several stages. Various methods have been previously used for the synthesis of silver nanoparticles, including sol–gel techniques, traditional chemical reduction, reverse micelle, co-precipitation, chemical vapour deposition, solvothermal, electrochemical reduction, ball milling [12–15], laser ablation [16], evaporation–condensation [17], electromagnetic levitation gas condensation [18], ultrasonication [19], lithography [20], and spray pyrolysis[21], radiolysis [22], arc discharge [23], and photoirradiation [24] were all previously employed to make silver nanoparticles. Previous investigations have employed a range of biological entities, including bacteria [25], fungi [26], viruses [27], yeasts [28], plants [29], plant extracts [30], microalgae [31], enzymes [32], saccharides [33], and vitamins [34]. The green synthesis of Ag nanoparticles has gained significant attention because of its cost-effectiveness, simplicity, scalability, environmental sustainability, and diverse array of plant-derived metabolites. Numerous herbal treatments have been employed in diverse medical systems to treat and manage various illnesses.

Bamboo plants have historically been employed in many traditional treatment systems to treat various human diseases. B. vulgaris is classified within the taxonomic family Poaceae. Bamboo leaves contain several flavonoids, such as homoorientin, orientin, isovitexin, vitexin, aringin-7-rhamnoglucoside, rutin, quercetin, luteolin, tricin, caffeic acid, chlorogenic acid, and hydroxycoumaric acid, as reported in previous studies [35, 36]. The plant under investigation has been documented to possess many phytochemical constituents, including carbohydrates, glycosides, saponins, alkaloids, flavonoids, phenolics and tannins, phytosterols, triterpenoids, oils, and lipids [37–39]. Studies have shown that silver nanoparticles produced from bamboo leaves have strong antibacterial effects on different types of bacteria. A study conducted by Jeyarambabu et al. demonstrated the use of Bambusaarundinacea leaf extract in the bio-fabrication of silver nanoparticles. This approach offers a promising and environmentally friendly alternative to the traditional chemical methods of producing Ag NPs. The AgNPs synthesized with the help of bamboo exhibited remarkable antibacterial effectiveness against both Gram-positive and Gram-negative pathogenic microorganisms. They demonstrated strong antioxidant activity against DPPH free radicals, indicating their potential as effective antioxidants. In addition, the Ag NPs exhibited strong anti-cancer properties against MCF-7 cell lines, suggesting their potential as a therapeutic agent [40]. The extract utilized in the preparation of silver nanoparticles has shown encouraging outcomes in reducing the organic pollutant methylene blue (MB). The silver nanoparticles (Ag-NPs) produced through the use of Cytobacillus firmus extract exhibited strong antibacterial and antifungal properties against a range of microorganisms, such as Escherichia coli, Enterococcus feacalis, Pseudomonas aeruginosa, Staphylococcus aureus, and Candida albicans. Ag-NPs exhibited a significant level of biodegradability (98%) for methylene blue (MB) dye within 8 h of co-incubation under sunlight. The

water sample contaminated with MB dye displayed promising results in terms of Vicia faba germination, suggesting that the purified water could be effectively reused for agricultural applications [41]. In a recent study, Rajeshree Patwari and her colleagues showcased their findings on synthesising silver nanoparticles (AgNPs) through the solution combustion synthesis (SCS) technique. This method led to the creation of well-defined, crystalline AgNPs at the nanoscale. The synthesised silver nanoparticles exhibit promising antimicrobial properties against various bacteria, including S. aureus, B. subtilis, P. aeruginosa, and E. coli. Among these, B. subtilis appears to be the most vulnerable to nanoparticle effects. The AgNPs also demonstrate exceptional photocatalytic activity in the degradation of indigo carmine dye [42]. In 2023, Muhammad Ateeb et al. conducted a study that focused on fabricating silver nanoparticles (AgNPs) using Grewia asiatica leaf extract. The researchers also analysed the optical and physicochemical properties of these nanoparticles. When exposed to visible light, agNPs demonstrated significant photocatalytic activity in deleting crystal violet dye. AgNPs exhibited significant antibacterial effects against gram-positive and gram-negative bacteria and notable anti-inflammatory and anti-arthritic properties. The utilisation of Grewia asiatica leaf extract in the synthesis of AgNPs offers a sustainable and environmentally conscious method for their production. The results emphasise the wide range of applications for AgNPs, both as a highly effective photocatalyst and as a valuable tool in the biomedical field [43]. The antibacterial properties of this substance are highly effective and have potential use in the pharmaceutical industry [44]. The evaporation flow and thermal stability are greatly enhanced by synthesising SiO_2 nanoparticles using bamboo leaf ash [45]. A comprehensive investigation of the non-toxicity mechanism of biosynthesised silver nanoparticles necessitates the use of bamboo leaf extract as a means to characterise their properties thoroughly. It is particularly relevant in their potential application in medical treatments to reduce blood sugar levels [46]. The current study involved the synthesis of ion-free silver nanoparticles using bamboo leaf extract. The reductions were achieved using compounds derived from an extract, which served as the reducing agent. Dyes play a significant role in both the printing and textile industries. Their effluent discharge was dispersed into the aquatic ecosystem, introducing pigmented substances and dye molecules resistant to degradation. The dissemination of dyestuffs contributes to the proliferation of numerous diseases on a global scale. Methylene blue is commonly employed in textile printing despite its known environmental toxicity and potential to induce carcinogenic illnesses. Several techniques exist for removing dye from the environment, including flocculation, redox reduction, adsorption, and photocatalysis [47–50]. Photocatalysis is a notable and efficient approach for eliminating organic compounds because of its convenience and compact nature. This study focused on analysing the structural, optical, and morphological properties of the synthesised silver nanoparticles. In addition, the photocatalytic endurance of these nanoparticles against the MB dye under visible light energy was observed.

2 Experimental section

2.1 Materials

The chemicals used in this study, namely silver nitrate ($AgNO_3$) and methylene blue dye, were obtained from HiMedia, a reputable supplier based in India. The compounds were processed and synthesised without undergoing purifying procedures. The solvent used in the experiment was double distilled water.

2.2 Preparation of the plant extract

The leaves of *B. vulgaris* were gathered in Tirunelveli, India. The leaves were subjected to a two-stage washing procedure, initially with flowing tap water followed by double distilled water, to remove any soil particles and foreign matter that may have been present. A quantity of 10 g of *B. vulgaris* leaves, which had undergone prior cleaning, was added to 100 mL of double distilled water. The mixture was subsequently heated to a temperature of 60 °C and maintained for 30 min. The extract underwent filtration using Whatman No: 1 filter paper. The resultant supernatant was then collected and stored at a temperature of 4 °C for future utilisation.

2.3 Synthesis of the Ag nanoparticles

10 ml of *B. vulgaris* leaf extract was mixed with 90 mL of a 0.1 M $AgNO_3$ solution. A magnetic stirring apparatus then agitated the solution at a uniform rotational velocity. The transparent liquid underwent a chemical change, forming a deep brown colour, which suggests the rapid formation of silver nanoparticles. The solution was treated to a washing process using double distilled water and subsequently underwent centrifugation at a speed of 5000 rpm for 10 min. The solution was filtered with Whatman No. 1 filter paper and dried in a hot air furnace at 100 °C for one hour. The collected samples were finely pulverised into a powdered form using a mortar and pestle, and this resulting powder was later employed for further characterisationendeavours.

2.4 Characterisation of the Ag nanoparticles

Structural evidence was obtained using an X-ray diffractometer (PANalytical X-Pert Pro-2θ range of 10°-80°), while morphological data were gathered using a transmission electron microscope named TEM, Philips CM200. The optical properties were determined using Fourier transform infrared spectroscopy (FTIR-Perkin Elmer-4000 cm-1 to 400 cm-1) and UV–visible spectrophotometry (PerkinElmer Lambda-35 UV–visible range from 200 to 800 nm). The luminescent properties were observed using a photoluminescence (PL) spectrofluorometer model PC1 manufactured by ISS in the United States. The surface characteristics and elemental composition were documented using scanning electron microscopy with energy-dispersive X-ray spectroscopy (SEM–EDX) conducted using a Carl Zeiss instrument.

2.5 Photocatalytic activity of the Ag nanoparticles

This study used silver nanoparticles to investigate the photocatalytic degradation of methylene blue dye, a representative model dye for textile dye pollution. The utilisation of visible light energy as a light source is achieved through a xenon lamp. The catalyst (10 mg) was initially suspended in a 100 cc MB dye solution. The catalyst was maintained in a dark environment for 60 min to achieve adsorption equilibrium. Subsequently, the solutions were introduced into a light chamber and subjected to continuous irradiation using a xenon lamp with a wavelength greater than 400 nm. The irradiation samples were periodically removed at 30-min intervals. The collected samples underwent centrifugation at a speed of 5000 rpm to separate the catalyst from the dye solution. In addition, the samples underwent filtration and were subjected to measurement using UV–Vis spectroscopy at a wavelength of 655 nm. The equation below determined the dye molecules' dissociation and efficiency.

$$\text{Photocatalytic dye degradation}(\%) = (\text{Co}-\text{Ct})/\text{Co} \times 100$$

where the primary dye concentration is Co (without irradiation) and the concentration of the dye at the reformed irradiation periods is Ct [51].

3 Results and discussion

3.1 UV–Vis spectral results

The confirmation of the formation of silver nanoparticles is evidenced by the observed colour transformation from a light green colour to a dark brown shade. The surface plasmon resonance scattering effect is well-organised at silver nanoparticles positioned at a wavelength of 450 nm, as depicted in Fig. 1 [52]. The absence of a peak in the valence silver can be attributed to the hindrance of electron movement from the conduction band due to the enormous size of its particles. The peaks observed at 0 min correspond to the initial interaction between the extract and silver nitrate solution. Upon initiating the interaction, it was observed that the *B. vulgaris* leaf extract facilitated the promotion of electrons, resulting in the oxidation and reduction of the silver nitrate solution. After 30 min, the reactions were concluded and verified by observing colour alterations. The absorbance of the completed reactions was found to be higher, resulting in a distinct peak compared with the reactions at 0 min, as illustrated in Fig. 1. The presence of a distinct peak indicated the development of silver nanoparticles with valence-free characteristics, whereas the broadening of the peak's breadth at half

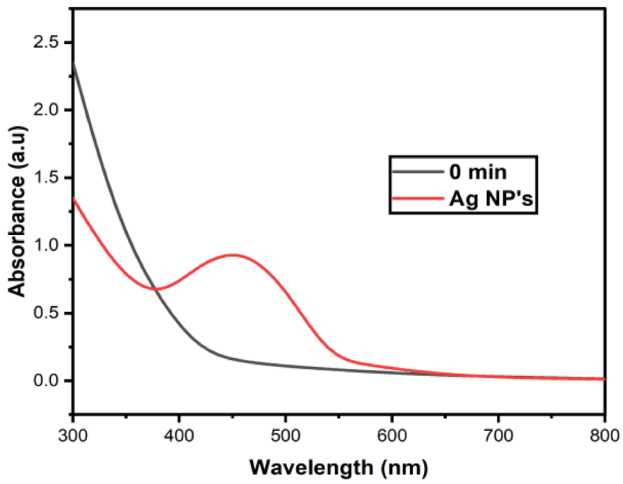

Fig. 1 UV –visible spectrum of the synthesised silver nanoparticles

maximum provided information about the size distribution of the particles. The *B. vulgaris* leaf extract may exert control and resistance over the nucleation and growth of nanoparticles through its ability to influence the size and dispersion of the particles [53]. The silver metal exhibits a significant increase in size at 0 min, and the presence of peaks corresponding to silver nanoparticles verifies the reduction of silver metal ions to form silver nanoparticles. Electron-mediated transmission of reactions was observed in the leaf extract of *B. vulgaris*. Furthermore, *B. vulgaris* leaf extract electrons have been observed in encapsulating the synthesised nanoparticles. This extract plays a crucial role in regulating the agglomeration of particles during the synthesis procedure and is responsible for their stabilisation.

3.2 FT-IR analysis

The chemical constituents accountable for reducing Ag + ions to Ag nanoparticles were investigated using FT-IR spectroscopy. The spectral analysis results obtained are depicted in Fig. 2. The wavenumber of 2846 cm^{-1} corresponds to the observation of a band, which is associated with the symmetric stretching of CH_3 groups [54]. The absorbance peak detected at 2343 cm^{-1} [55] in the leaf extract indicates the presence of hydroxyl functional groups of alcohols and phenolic substances. As reported in reference, the peak detected at a wavenumber of 1583 cm^{-1} is frequently linked to the N–H bending vibration of primary and secondary amines [56].The presence of two prominent peaks at 1312 cm^{-1} and 1152 cm^{-1} might be ascribed to the stretching vibrations of C–O and C–O–C bonds, respectively, as reported in previous studies [57, 58]. The peak prominent at a wavenumber of 1005 cm-1 is ascribed to the vibrational modes of the N–H bonds in primary and secondary amines [59]. The peak observed at 748 cm^{-1} is attributed to the vibrational mode of the –CN bond in the benzene ring [60]. Bamboo foliage comprises diverse bioactive constituents, such as flavonoids, glycosides, phenolic acids, coumarin lactones, anthraquinones, and amino acids [35]. The leaves possess phytochemical compounds

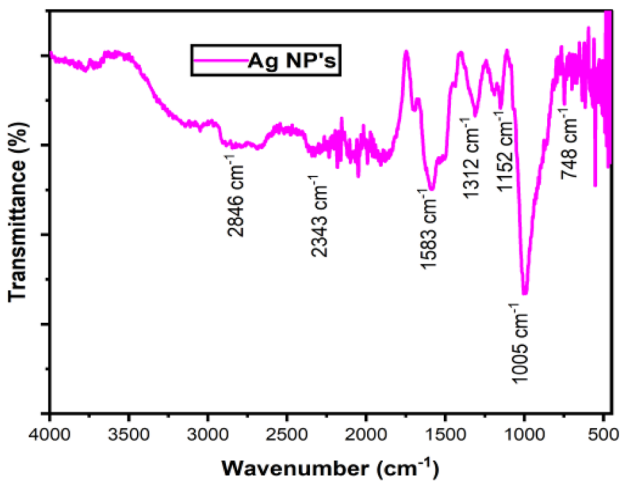

Fig. 2 FT-IR spectra of the synthesised silver nanoparticles

that have dual roles as reducing and capping agents during synthesis. In contrast to chemical reduction approaches, using leaf extract biomolecules to expedite reduction processes presents a more ecologically sustainable strategy. The reducing capabilities of flavonoids have been found, whereas the encapsulation of the synthesised nanoparticles is attributed to carboxylic and phenolic acids [61].

3.3 XRD analysis

X-ray diffractograms depicting the synthesised Ag nanoparticles through the use of Bambusa vulgaris leaf extract are presented in Fig. 3a and b. Crystallographic peaks were found at (111), (200), (220), and (311), with matching 2θ theta values of 38.09°, 44.06°, 64.25°, and 77.21°. The presence of plant phytomolecules is indicated by excess peaks in conjunction with silver [62, 63]. Plant-derived phytomolecules can serve as reducing agents, stabilisers, or both in nanoparticle production. The leaf extract phytomolecules may be possible reducing agents in forming silver nanoparticles, with the synthesised nanoparticles likely containing phytomolecules on their surface [62, 63]. Consequently, the centrifugation procedure was conducted iteratively, ranging from 7 to 8 repetitions, to exclude the presence of surplus plant-based substances that may have caused contamination. Furthermore, we have obtained a set of five unique diffraction standard peaks for silver at specific angles: 38.09º, 44.06º, 64.25º, 77.21º, and 81.11º. These angles correspond to their respective crystalline planes (111), (200), (220), (311), and (222), accordingly. The planes observed strongly resemble the face-centred

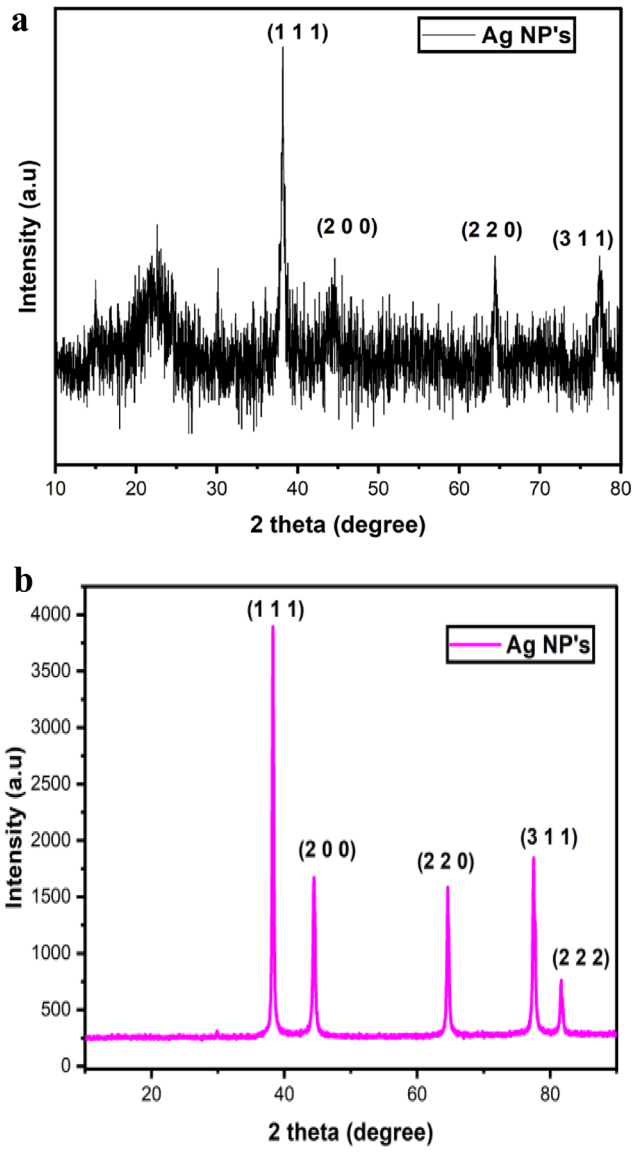

Fig. 3 **a** X-ray diffraction spectrum of the Ag nanoparticles before centrifugation. **b** X-ray diffraction spectrum of the Ag nanoparticles after centrifugation

cubic structure described in the JCPDS card no. 89–3722 [64]. The X-ray diffraction (XRD) pattern displays distinct and pronounced peaks, indicating that the Ag nanoparticles synthesised by reducing Ag^+ ions with *Bambusa vulgaris* leaf extract possess a crystalline structure. The peaks observed in the diffractogram correspond to the crystallisation of the silver nanoparticles, as indicated by the assignment. The average crystallite size of the synthesised Ag nanoparticles was determined by employing Debye –Scherrer's equation, yielding a value of 21 nm. The confirmation of nanoparticle production and the catalytic and enhanced surface areas of the synthesised nanoparticles was indicated by the presence of sharp and high-intensity crystalline peaks, as reported in reference [65].

3.4 Morphological analysis

Scanning and transmission electron microscopy were used to look at the morphological features of the synthesised silver nanoparticles. Figure 4a and b present scanning electron microscopyimages of Ag nanoparticles synthesised using *Bambusa vulgaris* leaf extract as a mediator. These images depict the surface morphology of the nanoparticles, which exhibit a spherical form. The presence of dark spots in the photographs visually indicates the presence of biomolecules. Figure 4d displays the silver nanoparticles' energy-dispersive X-ray (EDX) spectra. The presence of silver metal and its co-occurrence in the sample were verified using elemental analysis, which indicated that they originated from both the plant extract and the instrumental source. The prominent signal observed at 2.8 keV indicates the presence of silver within the obtained silver nanoparticles. Figure 4c displays TEM images ofsynthesised silver nanoparticles using *Bambusa vulgaris* leaf extract. The images reveal sphericalnanoparticles, which exhibit a polydisperse distribution. The particle distribution analysis indicated a substantial surface area and a homogeneous distribution across the surface [66]. The mean diameter of the synthesised nanoparticles typically falls within the range of approximately 22 nm. The confirmation and validation of the excited electron surface plasmon resonance (SPR) in the synthesised silver nanoparticles is provided by their spherical morphology, as observed through UV–Vis analysis. The enhanced photocatalytic activity of small-sized nanoparticles can be attributed to their increased surface area, which results in a more significant number

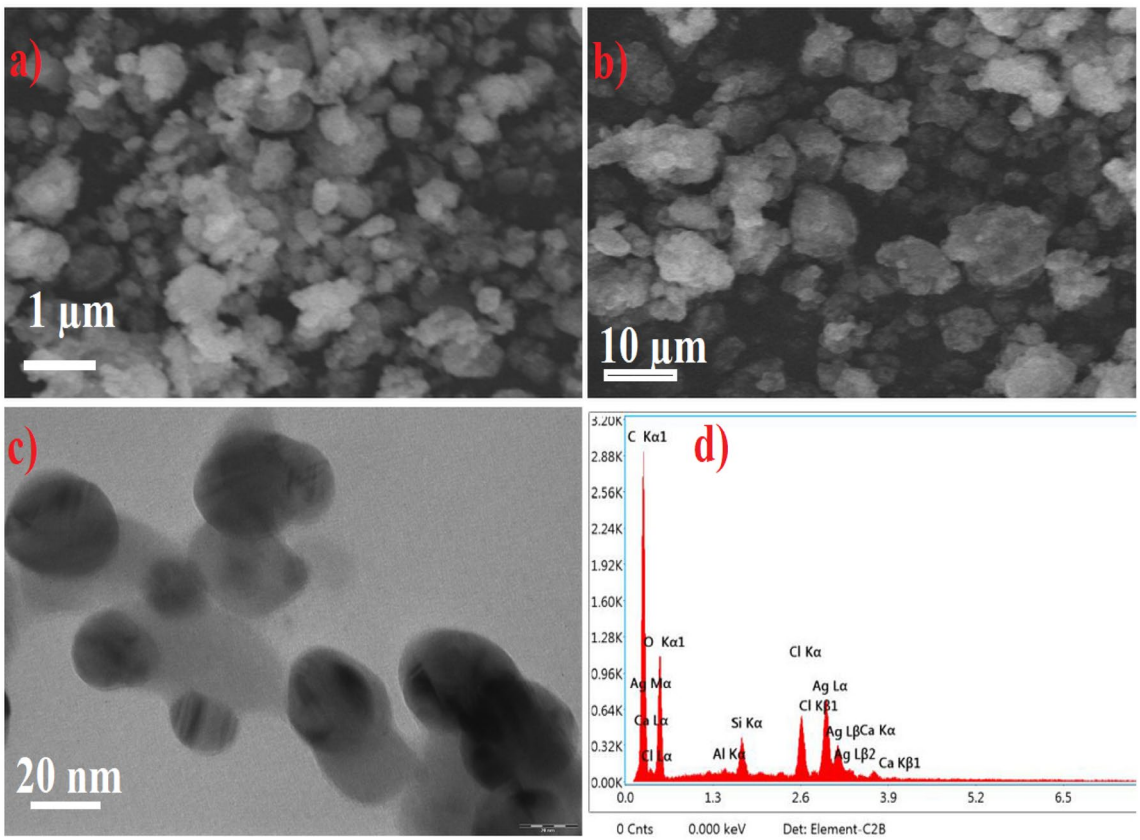

Fig. 4 **a**, **b** SEM, **c** TEM, and **d** EDX images of the synthesised silver nanoparticles

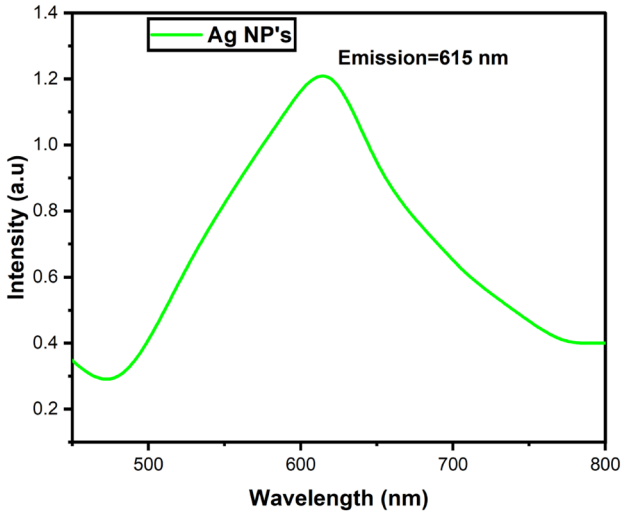

Fig. 5 Photoluminescence spectra of the synthesised silver nanoparticles

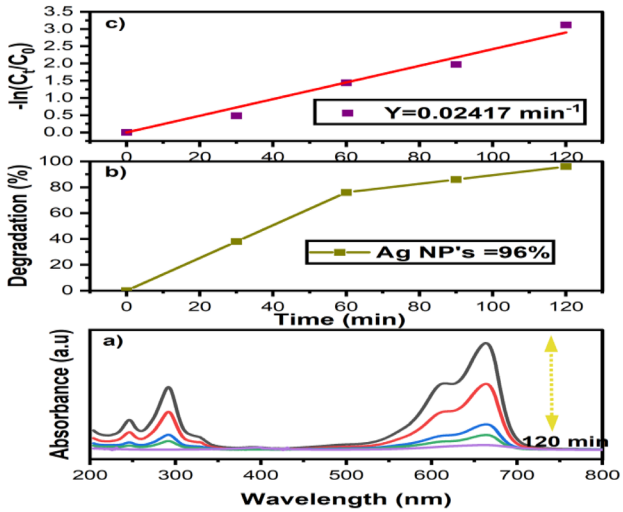

Fig. 6 **a**–**c** Photocatalytic dye degradation spectrum of Ag nanoparticles

of active sites on the nanoparticle surface [58–67]. In addition, a polydispersity attitude has been found to enhance the generation of hot electrons, contributing to improved photocatalytic performance.

3.5 Photoluminescence

Photoluminescence analysis was performed to investigate the optical characteristics of the silver nanomaterial. The excitation of silver nanoparticles occurs at a wavelength of 246 nm [68]. The emission peak observed at a wavelength of 645 nm corresponds to the yellow-green emission, as depicted in Fig. 5. Furthermore, the stimulation of electrons demonstrated the creation of silver nanoparticles, where the excited electrons transitioned from d bands to energy states that surpassed the Fermi level. Energy loss occurs during the scattering process between electron and hole phonons. This scattering process produces absorbed electrons and holes, stimulating the radiation recombination of sp electrons in silver nanoparticles [69]. Excited electrons and holes produce high-energy free radicals, contributing to the wide full width at half maximum (FWHM) observed in synthesised silver nanoparticles. The ability to control surface plasmon radiation is due to this property [70].

3.6 Photocatalytic activity

The photocatalytic efficacy of the silver nanoparticles was evaluated for the degradation of the methylene blue dye, as depicted in Fig. 6a–c. Dyes comprise numerous poisonous and carcinogenic chemicals that induce adverse health effects

in humans and other creatures. Photocatalytic activity encompasses converting light energy into chemical energy, which results in the creation of charge carriers. The first stage of dye degradation using a photocatalyst entails the migration of dye molecules onto the surface of the photocatalytic material. Moreover, after the degradation process, the dye molecule undergoes decomposition due to oxidised chemicals. The outcome exhibits no harmful effects on the environment. The $n-\pi^*$ transition exhibited a maximum absorbance peak at 665 nm [71]. A progressive decline in absorption spectra is noticed as the intensity of light irradiation increases. When exposed to visible light, the ultraviolet–visible (UV–Vis) spectra demonstrated a significant deterioration of 96% for methylene blue. The degradation kinetics was determined using a model based on pseudo-first-order kinetics, which can be characterised as follows:

$$-\ln\left(\frac{C_t}{C_0}\right) = -kt$$

The concentration of the MB dye at time t is denoted as Ct, while C0 represents the original MB dye concentration. The first-order rate constant, denoted by k, is the most intuitively apparent. The dye removal kinetics of the synthesised sample was determined to be 0.02417 min^{-1}.

The degradation mechanisms of the MB dye utilising Ag nanoparticles synthesised as a catalyst are illustrated in Fig. 7. The degradation pathway method is outlined as follows:

$$Ag + \text{light energy} \rightarrow V.B^{+} + C.B(e^{-}) \quad (1)$$

$$C.B(e^{-}) + O_2 \rightarrow O_2^{\bullet -} \quad (2)$$

$$O_2^{\bullet -} + H^{+} \rightarrow HO_2^{\bullet} \quad (3)$$

$$HO_2^{\bullet} + H^{+} \rightarrow OH + HO^{\bullet} \quad (4)$$

$$V.B^{+} + OH \rightarrow HO^{\bullet} \quad (5)$$

$$O_2^{\bullet -} / HO^{\bullet} + Dye^{\bullet +} \rightarrow \text{dissociation dye products} \quad (6)$$

When a catalyst is exposed to visible light, the photogenerated holes located at the valence band of the catalyst migrate toward the catalyst surface. Upon reaching the surface, these holes react with hydroxyl (OH-) groups that have been adsorbed onto the catalytic surfaces, forming OH* radicals. The electrons within the conduction band undergo a combination with O_2, leading to the formation of the O_2 radical. Both radicals facilitate the oxidation of organic molecules on the catalyst surface, forming intermediate organic compounds. Charge carriers are believed to be responsible

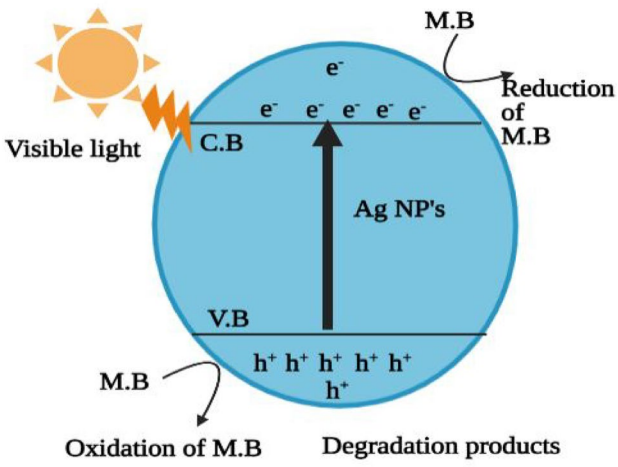

Fig. 7 Photocatalytic dye degradation mechanism of the silver nanoparticles

for the oxidation and reduction of dye molecules. The current study demonstrated a higher catalytic activity level than previously published research [72–76]. Moreover, it facilitates the chemical synthesis process and is an effective agent for wastewater treatment to eliminate organic pollutants.

3.6.1 Mechanism of photocatalytic degradation

The photocatalytic degradation process of methylene blue encompasses a series of sequential steps facilitated by the interplay between the photocatalyst and incident light energy. In the initial stage, methylene blue molecules' adsorption occurs on the photocatalyst's surface, which may consist of a semiconductor or a metal nanoparticle. The phenomenon of adsorption occurs because of electrostatic interactions and the inherent attraction between the catalyst surface and the MB molecule. When the photocatalyst is subjected to illumination, it absorbs photons possessing energy levels that surpass the bandgap of the catalyst. As a result, electron–hole pairs (e^- and h^+) formation occurs. The formation of holes, which are positively charged, occurs when electrons are excited from the valence band to the conduction band. The electrons and holes created by photoexcitation migrate toward the catalyst's surface. Electrons migrate toward surface regions with a more significant potential for reduction events, whereas holes migrate toward regions where oxidation reactions occur. The electrons created by light on the catalyst's surface engage in reduction processes by engaging with either adsorbed oxygen molecules or water molecules. This process generates highly oxidising reactive oxygen species (ROS) like superoxide radicals ($\bullet O_2^-$) and hydroxyl radicals (•OH). The reactive oxygen species (ROS) on the catalyst's surface initiate a chemical reaction with the adsorbed methylene blue molecules. Hydroxyl radicals (•OH) can extract hydrogen atoms from MB, generating intermediate intermediates. The intermediates generally exhibit reduced colouration and stability compared with the initial methylene blue molecule. The degradation process persists as these intermediate products interact with reactive oxygen species (ROS), breaking these molecules into smaller, less complex forms. The degradation ultimately results in the mineralisation of methylene blue molecules, forming benign byproducts, including carbon dioxide, water, and minute organic fragments. The products and byproducts that have undergone degradation are ultimately desorbed from the catalyst's surface because of alterations in the surrounding chemical environment. The particles are introduced into the solution, eliminating them from the system. The photocatalyst is not depleted during the procedure and can be restored. The recombination of trapped electrons and holes on the catalyst's surface facilitates the restoration of the catalyst to its initial condition, thus enabling it to undergo subsequent cycles of deterioration.

3.6.2 Effect of catalyst concentration

Figure 8 illustrates the impact of the catalyst dosage on the breakdown of MB. The degradation process of methylene blue can be controlled by multiple factors, one of which is the catalyst concentration. Within the framework of degradation reactions, catalysts can either augment or impede the degradation process, depending on the distinct catalyst and conditions of the reaction. Silver nanoparticles can facilitate the degradation of methylene blue when exposed to visible

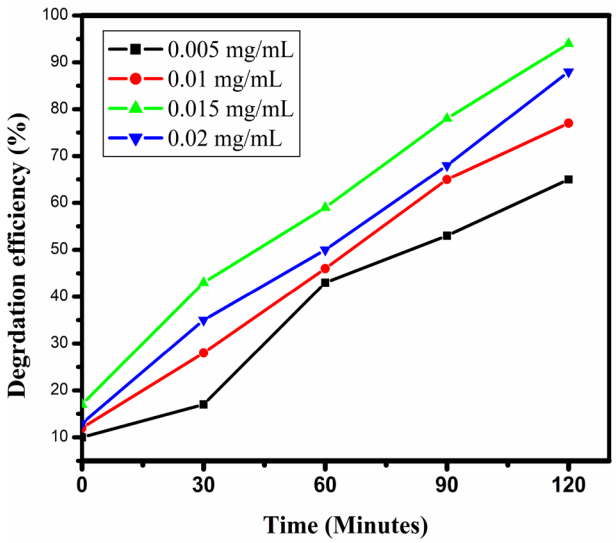

Fig. 8 The effect of catalyst dosage on the degradation of MB

Table 1 Shows degradation efficiency of silver nanoparticles

S. No	Nanoparticles	Biomaterials	Efficiency	Time	References
1	Ag	*Citrus reticulata*	100%	120 h (5 days)	[77]
2	Ag	Thespesia populnea Bark Extract	92%	123 Mins	[78]
3	Ag	cauliflower	97.57%	150 Mins	[79]
4	Ag	Chlorella vulgaris	96.51%	180 Mins	[80]
5	Ag	Camellia sinensis leaf	95%	72 h	[81]
6	Ag	Eupatorium adenophorum	78.69%	90 Mins	[82]
7	Ag	Bambusa vulgaris	94	120 Mins	Present work

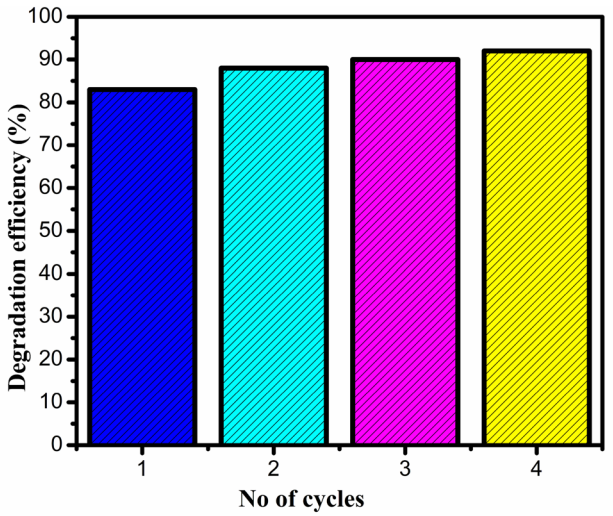

Fig. 9 The stability of silver nanoparticles after four cycles

light. Elevated concentrations of catalysts can enhance the degradation rate by offering a more significant number of active sites for adsorption and promoting the production of reactive oxygen species upon absorption of light. Nevertheless, an ideal catalyst concentration may exist, beyond which any additional increments may result in aggregation or shielding phenomena, ultimately diminishing the effectiveness of the catalyst. The user's statement outlines a research endeavour focused on the degradation of MB dye by implementing Ag Nanoparticles as a catalyst in the presence of solar irradiation. The study is presumed to have examined the impact of varying Ag NPs, ranging from 0.005 mg/mL to 0.02 mg/mL, on the degradation process over 120 min. The alterations in the degradation process were noticed through the use of UV–Vis absorption spectroscopy. UV–Vis absorption spectroscopy is a widely employed method for monitoring variations in the concentration of a chemical substance inside a solution by measuring light absorption at various wavelengths. No additional absorption peaks are observed over the entire procedure, thus verifying the complete breakdown of MB. Furthermore, the degradation pattern exhibits an initial increase in intensity with an increase in the dose of Ag nanoparticles but decreases beyond a dosage of 0.015 mg/mL. Significantly, an increased dose of Ag nanoparticles leads to pronounced opacity, mainly attributed to agglomeration, subsequently leading to enhanced light scattering. As a result, the level of sunlight penetration into the aqueous solution of MB is reduced because of cloudiness. Consequently, the effectiveness of photocatalysis significantly depends on the dosage of Ag. The degradation efficiencies of MB vary depending on the doses of Ag nanoparticles, with recorded values of 65%, 77%, 94%, and 88%, respectively. Table 1 shows degradation efficiency of silver nanoparticles compared with other materials.

3.6.3 Reusability of the catalyst

Figure 9 illustrates the stability of the silver nanoparticles following four cycles. This study assessed the long-term durability and potential for reliability of the finely tuned Ag photocatalyst (at a concentration of 0.015 mg/mL) in the degradation of MB dye using an optimised concentration of 10 µM. This evaluation was conducted over four cycles of sunlight exposure, as depicted in Fig. 9. In every iteration, it is necessary to maintain a constant concentration of MB dye, and the catalyst obtained through centrifugation is utilised for subsequent degradation rounds.

Table 2 Antibacterial zone of inhibition for silver nanoparticles

Name of the bacteria	Control	Antibacterial activity zone of inhibition (mm)				
		KL1	KL2	KL3	KL4	KL5
Pseudomonas aeruginosa	Amikacin	12	14	16	13	13
Staphylococcus aureus		18	16	21	14	16

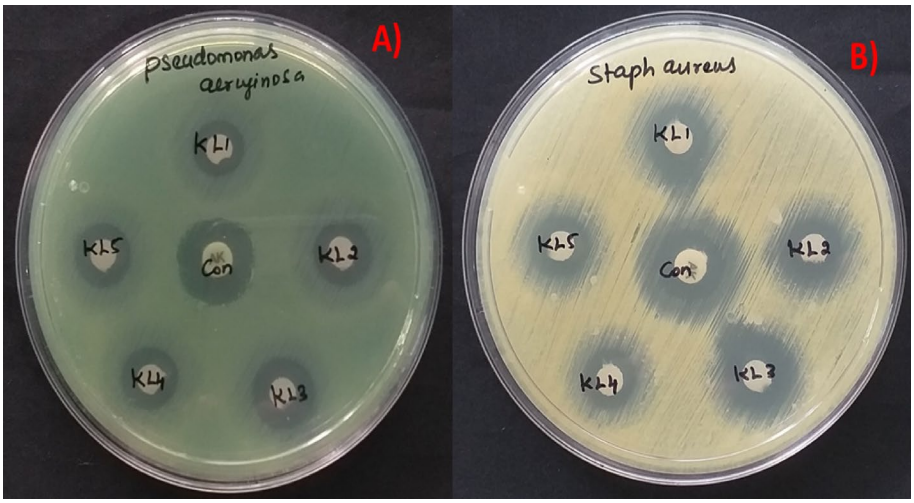

Fig. 10 Image of the antibacterial zone of inhibition for silver NPs

After undergoing four iterations, the catalyst exhibits impressive performance and demonstrates notable resilience against degradation driven by light. The RB dye exhibits its most significant degradation after 60 min, yielding 83%, 85%, 90%, and 91% efficiencies for the initial, second, third, and fourth cycles, respectively.

3.7 Antibacterial activity

The chemical exhibits antibacterial activity, which refers to its capacity to eradicate or inhibit the proliferation of microorganisms, thus impeding their ability to replicate. The activity exhibited by the nanoparticles can be attributed to various factors, including the synergistic impact resulting from their combined action, the nuclearity of the molecule, the specific coordination nature of the compounds involved, and the creation of chelates. The Kirby-Bauer disk diffusion method was employed to assess the antibacterial efficacy of nanoparticles. In this experimental procedure, nutritional agar was employed as a culture medium and carefully placed onto a Petri dish with a diameter of 85 mm, reaching a uniform depth of 4 mm. The pH of the medium is maintained within the range of 7.2 to 7.4. The agar media is subsequently inoculated with the chosen bacteria through streaking, where a cotton swab containing the pathogen is swiped across the agar surface in multiple directions. In addition, 6-mm filter paper disks saturated with the appropriate concentration of the prepared samples were systematically positioned on the agar media. The Petri dishes were incubated at 35 to 37 °C for 24 h in a controlled environment. The formation of zones occurs after a specific duration and is quantified within a range of millimetres to determine the antibacterial efficacy of the nanoparticles.

The results of the inhibition zone for silver nanoparticles (NPs) are presented in Table 2. It is evident from the data that the developed material exhibits enhanced resistance against the gram-positive bacterium *Staphylococcus aureus*, with the silver NPs displaying the largest zone of inhibition. Staphylococcus aureus exhibits a more significant zone of inhibition than *Pseudomonas aeruginosa*, which can be attributed to the differential concentration of positively and negatively charged ions within both bacterial species. The antibacterial activity of silver nanoparticles is enhanced against the gram-negative bacteria *Pseudomonas aeruginosa* and *Staphylococcus aureus*. Figure 10 displays pictures that depict the zone of inhibition.

4 Conclusion

There has been an increasing emphasis on sustainable technological advancements, driven by concerns about significant pollution and global warming shortly. Addressing the issue of removing pollutants from water sources comes with challenges, primarily stemming from the considerable amount of chemicals needed for photocatalyst preparations. Thus, it was discovered that producing biomolecules is more advantageous when creating nanomaterials. During our research, we conducted a study where we successfully synthesised silver nanoparticles using an extract from Bambusa vulgaris leaves. Our research has shown that these nanoparticles effectively remove organic pollutants from water. Based on the structural-based PXRD characterisation, it can be observed that the 2θ values are 38.09, 44.06, 64.25, and 77.21°. This provides evidence that the silver nanoparticles synthesised have a face-centred cubic structure. The grain sizes obtained from the PXRD pattern analysis using the Debye–Scherrer equation resulted in a measurement of 21 nm. The UV–Vis spectra show a distinct peak at 450 nm, indicating the SPR effect of Ag nanoparticles. The FT-IR measurement reveals that the biomolecules present in the extracts are located on the surface of the Ag nanoparticles, resulting in a significant reduction in particle size. Through careful morphological investigations, it was observed that there were random particles present on the surface. Consequently, it exhibits a surface with varying particle sizes. The TEM results indicate that the silver particles synthesised have a spherical shape and an average size of 22 nm. After conducting thorough experimentation, it was observed that the silver particle successfully reduced the ad methylene blue organic pollutant. The degradation efficiency reached 96% after 120 min of visible light illumination. Furthermore, it demonstrates enhanced photostability and reusability following four consecutive cycles. The findings demonstrate the potential for advancing wastewater treatment applications and exploring new instruments in this field.

Acknowledgements This project was supported by Researchers Supporting Project Number (RSP-2024R7) King Saud University, Riyadh, Saudi Arabia.

Author contributions Manuscript was written, Sample preparation, characterization was done by SSP. SAF and MA performed the XRD measurement, and the partial involvement of the draft of the manuscript. PRK and MS did the proofreading. CH performed overall supervision of work and was involved in manuscript write-up.

Funding The authors have not disclosed any funding.

Data availability The datasets generated and analysed during the current study are available from the corresponding author upon reasonable request.

Declarations

Ethical approval and consent to participate All experiments followed university guidelines. None of the authors used human beings as research subjects.

Consent for publication In this study; there was no personal data.

Competing interests The authors declare no conflicts of interest.

References

1. Cuong HN, Pansambal S, Ghotekar S, Oza R, Hai NTT, Viet NM, Nguyen VH. New frontiers in the plant extract mediated biosynthesis of copper oxide (CuO) nanoparticles and their potential applications: a review. Environ Res. 2022;203:111858.
2. Pandit C, Roy A, Ghotekar S, Khusro A, Islam MN, Emran TB, Bradley DA. Biological agents for synthesis of nanoparticles and their applications. J King Saud Univ Sci. 2022;34(3):101869.
3. Ghotekar S, Pansambal S, Pawar SP, Pagar T, Oza R, Bangale S. Biological activities of biogenically synthesized fluorescent silver nanoparticles using Acanthospermum hispidum leaves extract. SN Appl Sci. 2019;1:1–12.

4. Kashid Y, Ghotekar S, Bilal M, Pansambal S, Oza R, Varma RS, Mane D. Bio-inspired sustainable synthesis of silver chloride nanoparticles and their prominent applications. J Indian Chem Soc. 2022;99(5):100335.
5. Ghotekar S, Pagar K, Pansambal S, Murthy HA, Oza R. Biosynthesis of silver sulfide nanoparticle and its applications. In: Handbook of greener synthesis of nanomaterials and compounds. Amsterdam: Elsevier; 2021. p. 191–200.
6. Amina M, Al Musayeib NM, Alarfaj NA, El-Tohamy MF, Oraby HF, Al Hamoud GA, Moubayed NM. Biogenic green synthesis of MgO nanoparticles using Saussureacostus biomasses for a comprehensive detection of their antimicrobial, cytotoxicity against MCF-7 breast cancer cells and photocatalysis potentials. PLoS ONE. 2020;15(8):e0237567.
7. Amendola V, Pilot R, Frasconi M, Marago OM, Iatì MA. Surface plasmon resonance in gold nanoparticles: a review. J Phys Condens Matter. 2017;29(20):203002.
8. Stupar RM. Into the wild: the soybean genome meets its undomesticated relative. Proc Natl Acad Sci. 2010;107(51):21947–8.
9. Boisselier E, Astruc D. Gold nanoparticles in nanomedicine: preparations, imaging, diagnostics, therapies and toxicity. Chem Soc Rev. 2009;38(6):1759–82.
10. Berekaa MM. Nanotechnology in food industry; advances in food processing, packaging and food safety. Int J Curr Microbiol App Sci. 2015;4(5):345–57.
11. HuL CY. Energy and environmental nanotechnology in conductive paper and textiles. Energy Environ Sci. 2012;5(4):6423–35.
12. Khayati GR, Janghorban K. An investigation on the application of process control agents in the preparation and consolidation behavior of nanocrystalline silver by mechanochemical method. Adv Powder Technol. 2012;23(6):808–13.
13. Khayati GR, Janghorban K. The nanostructure evolution of Ag powder synthesised by high energy ball milling. Adv Powder Technol. 2012;23(3):393–7.
14. Jayaramudu T, Raghavendra GM, Varaprasad K, Reddy GVS, Reddy AB, Sudhakar K, Sadiku ER. Preparation and characterisation of poly (ethylene glycol) stabilised nano silver particles by a mechanochemical assisted ball mill process. J Appl Polym Sci. 2016;133(7):43027.
15. Boutinguiza M, Comesaña R, Lusquiños F, Riveiro A, Del Val J, Pou J. Production of silver nanoparticles by laser ablation in open air. Appl Surf Sci. 2015;336:108–11.
16. Verma S, Rao BT, Srivastava AP, Srivastava D, Kaul R, Singh B. A facile synthesis of broad plasmon wavelength tunable silver nanoparticles in citrate aqueous solutions by laser ablation and light irradiation. Colloids Surf, A. 2017;527:23–33.
17. BakerC PA, Paktis L, Pochan DJ, Shah SI. Antimicrobial activity of silver nanoparticles. J J Nanosci Technol. 2005;5:244–9.
18. Hui KS, Hui KN, Dinh DA, Tsang CH, Cho YR, Zhou W, Chun HH. Green synthesis of dimension-controlled silver nanoparticle–graphene oxide with in situ ultrasonication. Acta Mater. 2014;64:326–32.
19. Park M, Sohn Y, Shin WG, Lee J, Ko SH. Ultrasonication assisted production of silver nanowires with low aspect ratio and their optical properties. 2015.
20. Wu J, Zan X, Li S, Liu Y, Cui C, ZouB HF. In situ synthesis of large-area single sub-10 nm nanoparticle arrays by polymer pen lithography. Nanoscale. 2014;6(2):749–52.
21. Jang HD, Kim SK, Chang H, Jo EH, Roh KM, Choi JH, Choi JW. Synthesis of 3D silver-graphene-titanium dioxide composite via aerosol spray pyrolysis for sensitive glucose biosensor. Aerosol Sci Technol. 2015;49(7):538–46.
22. Juby KA, Dwivedi C, Kumar M, Kota S, Misra HS, Bajaj PN. Silver nanoparticle-loaded PVA/gum acacia hydrogel: Synthesis, characterisation and antibacterial study. Carbohyd Polym. 2012;89(3):906–13.
23. Kumar P, Singh PK, Hussain M, Kumar Das A. Synthesis of silver metal nanoparticles through electric arc discharge method: a review. Adv Sci Lett. 2016;22(1):3–7.
24. Zhang JD, Yu M, Liu JH, Li SM, Meng YB. Effect of Plasmid DNA Dimension Evolution on the Size of Ag Nanoparticles during Photoirradiation. In: Materials Science Forum, vol. 847. Switzerland: Trans Tech Publications Ltd; 2016. p. 194–9.
25. Li X, Kim N, Youn S, An TK, Kim J, Lim S, Kim SH. Sol–gel-processed organic-inorganic hybrid for flexible conductive substrates based on gravure-printed silver nanowires and graphene. Polymers. 2019;11(1):158.
26. Zhu J, Xu X, Liu J, Zheng Y, Hou S. Facile synthesis of oleylamine-capped silver nanowires and their application in transparent conductive electrodes. RSC Adv. 2015;5(90):74126–31.
27. Ciobanu CS, IconaruSL CMC, Costescu A, Le Coustumer P, PredoiD,. Synthesis and antimicrobial activity of silver-doped hydroxyapatite nanoparticles. BioMed Res Int. 2013;2013:916218.
28. Kaabipour S, Hemmati S. A review on the green and sustainable synthesis of silver nanoparticles and one-dimensional silver nanostructures. Beilstein J Nanotechnol. 2021;12(1):102–36.
29. Kuzminova A, Beranová J, Polonskyi O, Shelemin A, Kylián O, Choukourov A, Biederman H. Antibacterial nanocomposite coatings produced by means of gas aggregation source of silver nanoparticles. Surface Coatings Technol. 2016;294:225–30.
30. Chen D, Qiao X, Qiu X, Chen J, Jiang R. Large-scale synthesis of silver nanowires via a solvothermal method. J Mater Sci Mater Electron. 2011;22(1):6–13.
31. Nasretdinova GR, Fazleeva RR, Mukhitova RK, Nizameev IR, Kadirov MK, Ziganshina AY, Yanilkin VV. Electrochemical synthesis of silver nanoparticles in solution. Electrochem Commun. 2015;50:69–72.
32. Saravanan C, Rajesh R, Kaviarasan T, Muthukumar K, Kavitake D, Shetty PH. Synthesis of silver nanoparticles using bacterial exopolysaccharide and its application for degradation of azo-dyes. Biotechnol Rep. 2017;15:33–40.
33. MaL SuW, Liu JX, ZengXX HZ, Li W, Tang JX. Optimisation for extracellular biosynthesis of silver nanoparticles by Penicillium aculeatum Su1 and their antimicrobial activity and cytotoxic effect compared with silver ions. Mater Sci Eng C. 2017;77:963–71.
34. Fernández JG, Fernández-Baldo MA, Berni E, Camí G, Durán N, Raba J, Sanz MI. Production of silver nanoparticles using yeasts and evaluation of their antifungal activity against phytopathogenic fungi. Process Biochem. 2016;51(9):1306–13.
35. Dahoumane SA, Mechouet M, Wijesekera K, Filipe CD, Sicard C, Bazylinski DA, Jeffryes C. Algae-mediated biosynthesis of inorganic nanomaterials as a promising route in nanobiotechnology–a review. Green Chem. 2017;19(3):552–87.
36. Abdel-Raouf N, Al-Enazi NM, Ibraheem IBM, Alharbi RM, Alkhulaifi MM. Biosynthesis of silver nanoparticles by using of the marine brown alga Padina pavonia and their characterisation. Saudi J Biol Sci. 2019;26(6):1207–15.
37. Ayeni MJ, Oyeye MSD, Kayode J, Abanikanda AI. Phytochemical, Proximate and Mineral Analyses of the Leaves of Bambusa vulgaris L. and Artocarpus Altilis L. Ghana J Sci. 2018;59:69–77.

38. Fitri A, Asra R, RivaiH (2020) Overview of the traditional, phytochemical, and pharmacological uses of gold bamboo (BAMBUSA VULGARIS).
39. Owolabi MS, Lajide L. Preliminary phytochemical screening and antimicrobial activity of crude extracts of Bambusa vulgaris Schrad. Ex JC Wendl.(Poaceae) from southwestern Nigeria. Am J Essential Oils Nat Prod. 2015;3(1):42–5.
40. Jayarambabu N, Velupla S, Akshaykranth A, Anitha N, Rao TV. Bambusa arundinacea leaves extract-derived Ag NPs: evaluation of the photocatalytic, antioxidant, antibacterial, and anticancer activities. Appl Phys A. 2023;129(1):13.
41. Saied E, Hashem AH, Ali OM, Selim S, Almuhayawi MS, Elbahnasawy MA. Photocatalytic and antimicrobial activities of biosynthesized silver nanoparticles using Cytobacillus firmus. Life. 2022;12(9):1331.
42. Patwari DR, Swetha BN, Gurushantha K, Shobha G, Srinatha N, Mushrif SK, Keshavamurthy K. Photocatalytic and antimicrobial activities of biofunctionalized Ag nanoparticles derived from combustion method. Results Opt. 2023;12:100472.
43. Ateeb M, Asif HM, Ali T, Baig MM, Arif MU, Farooq MI, Shaukat I. Photocatalytic and Antibacterial activities of bio-synthesised silver nanoparticles (AgNPs) using Grewia asiatica leaves extract. Int J Environ Anal Chem. 2023. https://doi.org/10.1080/03067319.2022.2158328.
44. Yasi S, Liu L, Yao J. Biosynthesis of silver nanoparticles by bamboo leaves extract and their antimicrobial activity. J Fiber Bioeng Inform. 2013;6(6):77–84.
45. Kalita C, Ganguly M, Devi A. Biosynthesis of silver nanoparticles by using edible bamboo shoots with high antioxidant properties. Life Sci. Info Pub, 2018;4.
46. SethyNK AZ, Mishra PK, Kumar P. Synthesis of SiO2 nanoparticle from bamboo leaf and its incorporation in PDMS membrane to enhance its separation properties. J Polym Eng. 2019;39(7):679–87.
47. Anand A, Rao H, KunderNU BMP. Bio synthesis and characterization of silver nanoparticles by leaf extract of bamboo leaf and their antibacterial activity. Asian J Appl Sci Technol (AJAST). 2021;5(1):01–9.
48. Saratale RG, Saratale GD, Chang JS, Govindwar SP. Bacterial decolorisation and degradation of azo dyes: a review. J Taiwan Inst Chem Eng. 2011;42(1):138–57.
49. Al-Mamun MR, Kader S, Islam MS, Khan MZH. Photocatalytic activity improvement and application of UV-TiO2 photocatalysis in textile wastewater treatment: a review. J Environ Chem Eng. 2019;7(5):103248.
50. Nasir AM, Jaafar J, Aziz F, Yusof N, Salleh WNW, Ismail AF, Aziz M. A review on floating nanocomposite photocatalyst: fabrication and applications for wastewater treatment. J Water Process Eng. 2020;36:101300.
51. Sarafraz MM, Safaei MR, GoodarziM AM. Reforming of methanol with steam in a micro-reactor with Cu–SiO_2 porous catalyst. Int J Hydrogen Energy. 2019;44(36):19628–39.
52. Azeez L, Lateef A, Adebisi SA, Oyedeji AO. Novel biosynthesised silver nanoparticles from cobweb as adsorbent for Rhodamine B: equilibrium isotherm, kinetic and thermodynamic studies. Appl Water Sci. 2018;8(1):1–12.
53. Mulvaney P. Surface plasmon spectroscopy of nanosized metal particles. Langmuir. 1996;12(3):788–800.
54. Manosalva N, Tortella G, Diez MC, Schalchli H, Seabra AB, Durán N, Rubilar O. Green synthesis of silver nanoparticles: effect of synthesis reaction parameters on antimicrobial activity. World J Microbiol Biotechnol. 2019;35(6):1–9.
55. Mohan AN, Manoj B. Synthesis and characterisation of carbon nanospheres from hydrocarbon soot. Int J Electrochem Sci. 2012;7(10):9537–49.
56. Ashokkumar T, Arockiaraj J, Vijayaraghavan K. Biosynthesis of gold nanoparticles using green roof species Portulaca grandiflora and their cytotoxic effects against C6 glioma human cancer cells. Environ Prog Sustain Energy. 2016;35(6):1732–40.
57. Vidhya E, Vijayakumar S, PrathipkumarS PPK. Green way biosynthesis: characterisation, antimicrobial and anticancer activity of ZnO nanoparticles. Gene Rep. 2020;20:100688.
58. Philip D. Honey mediated green synthesis of silver nanoparticles. Spectrochimica Acta Part A Mol Biomol Spectrosc. 2010;75(3):1078–81.
59. Priyadarshini S, MainalA SF, Yahya R, Alyousef AA, Mohammed A. Biosynthesis of TiO 2 nanoparticles and their superior antibacterial effect against human nosocomial bacterial pathogens. Res Chem Intermed. 2020;46(2):1077–89.
60. Ethiraj AS, Jayanthi S, Ramalingam C, Banerjee C. Control of size and antimicrobial activity of green synthesised silver nanoparticles. Mater Lett. 2016;185:526–9.
61. Li Y, Kong D, Lin X, Xie Z, Bai M, Huang S, Wu H. Quality evaluation for essential oil of Cinnamomum verum leaves at different growth stages based on GC–MS, FTIR and microscopy. Food Anal Methods. 2016;9(1):202–12.
62. Yilmaz M, Turkdemir H, Kilic MA, BayramE CA, MeteA UlugB. Biosynthesis of silver nanoparticles using leaves of Stevia rebaudiana. Mater Chem Phys. 2011;130(3):1195–202.
63. Philip D. Biosynthesis of Au, Ag and Au–Ag nanoparticles using edible mushroom extract. Spectrochimica Acta Part A Mol Biomol Spectrosc. 2009;73(2):374–81.
64. Shankar SS, Ahmad A, Sastry M. Geranium leaf assisted biosynthesis of silver nanoparticles. Biotechnol Progress. 2003;19(6):1627–31.
65. Kumar VA, Uchida T, Mizuki T, NakajimaY KY, Hanajiri T, Maekawa T. Synthesis of nanoparticles composed of silver and silver chloride for a plasmonic photocatalyst using an extract from a weed Solidago altissima (goldenrod). Adv Nat Sci Nanosci Nanotechnol. 2016;7(1):015002.
66. Mao Z, Vang H, Garcia A, Tohti A, Stokes BJ, Nguyen SC. Carrier diffusion—the main contribution to size-dependent photocatalytic activity of colloidal gold nanoparticles. ACS Catal. 2019;9(5):4211–7.
67. LiD SH, MengX ShenT, Sun J, Han W, Wang X. Effects of particle size on the structure and photocatalytic performance by alkali-treated TiO_2. Nanomaterials. 2020;10(3):546.
68. Lateef A, Adelere IA, Gueguim-Kana EB, Asafa TB, Beukes LS. Green synthesis of silver nanoparticles using keratinase obtained from a strain of Bacillus safensis LAU 13. Int Nano Lett. 2015;5(1):29–35.
69. Hamzah M, Khenfouch M, Srinivasu VV. The quenching of silver nanoparticles photoluminescence by graphene oxide: spectroscopic and morphological investigations. J Mater Sci Mater Electron. 2017;28(2):1804–11.
70. Balaz M, Balazova L, Daneu N, Dutkova E, BalazovaM BZ, Shpotyuk Y. Plant-mediated synthesis of silver NPs and their stabilisation by wet stirred media milling, Baláž et al. Nanoscale Res Lett. 2017;12:83.
71. Aravind M, AhmadA AI, Amalanathan M, Naseem K, Mary SMM, ZuberM,. Critical green routing synthesis of silver NPs using jasmine flower extract for biological activities and photocatalytical degradation of methylene blue. J Environ Chem Eng. 2021;9(1):104877.

72. Vanaja M, Paulkumar K, Baburaja M, Rajeshkumar S, Gnanajobitha G, Malarkodi C, Annadurai G. Degradation of methylene blue using biologically synthesised silver nanoparticles. Bioinorg Chem Appl, 2014;2014.
73. Kumari RM, Thapa N, Gupta N, KumarA NS. Antibacterial and photocatalytic degradation efficacy of silver nanoparticles biosynthesised using Cordia dichotoma leaf extract. Adv Nat Sci Nanosci Nanotechnol. 2016;7(4):045009.
74. MominB RS, JhaN AUS. Valorisation of mutant Bacillus licheniformis M09 supernatant for green synthesis of silver nanoparticles: photocatalytic dye degradation, antibacterial activity, and cytotoxicity. Bioprocess Biosyst Eng. 2019;42(4):541–53.
75. Patel K, Abhale Y, Oza R, Lin KYA, Larios AP, Ghotekar S. Green Silver Nanoparticles for Nanoremediation. In: Green Nanoremediation: Sustainable Management of Environmental Pollution. Cham: Springer International Publishing; 2023. p. 253–74.
76. Ghotekar S, Savale A, Pansambal S. Phytofabrication of fluorescent silver nanoparticles from Leucaena leucocephala L. leaves and their biological activities. J Water Environ Nanotechnol. 2018;3(2):95–105.
77. Jaast S, Grewal A. Green synthesis of silver nanoparticles, characterization and evaluation of their photocatalytic dye degradation activity. Current Res Green Sustain Chem. 2021;4:100195.
78. Chopra HK. Tree bark and their role in nanomaterials synthesis and applications. Secondary Metabolites Based Green Synthesis of Nanomaterials and Their Applications, 2023;291.
79. Kadam J, Dhawal P, Barve S, Kakodkar S. Green synthesis of silver nanoparticles using cauliflower waste and their multifaceted applications in photocatalytic degradation of methylene blue dye and Hg 2+ biosensing. SN Appl Sci. 2020;2:1–16.
80. Rajkumar R, Ezhumalai G, Gnanadesigan M. A green approach for the synthesis of silver nanoparticles by Chlorella vulgaris and its application in photocatalytic dye degradation activity. Environ Technol Innov. 2021;21:101282.
81. Trieu QA, Le CTB, Pham CM, Bui TH. Photocatalytic degradation of methylene blue and antibacterial activity of silver nanoparticles synthesized from Camellia sinensis leaf extract. J Exp Nanosci. 2023;18(1):2225759.
82. Dua TK, Giri S, Nandi G, Sahu R, Shaw TK, Paul P. Green synthesis of silver nanoparticles using Eupatorium adenophorum leaf extract: characterizations, antioxidant, antibacterial and photocatalytic activities. Chemical Papers, 2023;1–10.